HOKKAIDO UNIVERSITY

Title	Nanomorphological changes of anodic aluminum oxide fabricated by anodizing in various phosphate solutions over a wide pH range
Author(s)	Terashima, Ayasa; Iwai, Mana; Kikuchi, Tatsuya
Citation	Applied surface science, 605, 154687 https://doi.org/10.1016/j.apsusc.2022.154687
Issue Date	2022-12-15
Doc URL	https://hdl.handle.net/2115/93009
Rights	© <2022>. This manuscript version is made available under the CC-BY-NC-ND 4.0 license https://creativecommons.org/licenses/by-nc-nd/4.0/
Rights(URL)	https://creativecommons.org/licenses/by-nc-nd/4.0/
Type	journal article
File Information	Phosphate.pdf

Hokkaido University Collection of Scholarly and Academic Papers : HUSCAP

Nanomorphological changes of anodic aluminum oxide fabricated by anodizing in various phosphate solutions over a wide pH range

Ayasa Terashima, Mana Iwai, Tatsuya Kikuchi*

Faculty of Engineering, Hokkaido University, N13-W8, Kita-ku, Sapporo, Hokkaido, 060-8628, Japan

*Corresponding author: Tatsuya Kikuchi
e-mail: kiku@eng.hokudai.ac.jp

Abstract

High-purity aluminum plates were anodized in phosphoric acid and six phosphate solutions over a wide pH range from acidic to alkaline. The current density corresponding to the growth rate of the anodic oxide was minimum when anodizing in near-neutral solutions and increased when the pH value increased or decreased. A typical porous anodic aluminum oxide (PAAO) film consisting of an outer porous layer and inner hemispherical barrier layer, which is based on the Keller–Hunter–Robinson (KHR) model, was formed in acidic solutions. At the pH values closer to the neutral region, a uniform barrier oxide film or a PAAO film with a narrow porous layer was produced owing to the low solubility of aluminum oxide. On the other hand, two types of characteristic PAAO films were formed during anodizing in alkaline phosphate solutions: one was a PAAO film consisting of an outer porous layer with feathered pore walls and inner hemispherical barrier layer, and the second was a PAAO film consisting of an outer porous layer with elongated pores and inner flat barrier layer. We showed that novel PAAO films, which are not based on the KHR model, can be prepared by anodizing aluminum in various alkaline phosphate solutions.

Keywords: Anodizing aluminum; Anodic Aluminum Oxide; Morphology; Phosphate; pH

1. Introduction

Porous anodic aluminum oxide (PAAO) films are typically fabricated via anodizing (anodization) of aluminum in several types of electrolyte solutions [1-5]. The nanomorphology of PAAO films was first revealed by Keller, Hunter, and Robinson (KHR) using an electron microscope in 1953 [6]. They found that PAAO films have a honeycomb-like structure consisting of numerous high-aspect-ratio hexagonal cells with a nanoscale pore in the center of each hexagonal cell. A thin hemispherical barrier layer at the bottom of each nanopore separates the aluminum substrate from the environment. The regularity of the hexagonal cells and pores formed in the PAAO film depends on the anodizing conditions. In mid- to late 1990s, Masuda et al. found that an ideally ordered PAAO film grows during potentiostatic anodizing under specific self-ordering conditions [7-9]. The interpore distance and pore diameter of the PAAO film can be precisely controlled by the appropriate choice of anodizing conditions, electrolyte, and post-treatment [10-13]. Based on these findings, the fabrication of various nanomaterials, such as metal-, oxide-, and polymer nanofibers [14-16], plasmonic devices [17,18], photonic crystals [19,20], nanocapacitors [21], structural color materials [22], nanoparticle arrays [23,24], and three-dimensional porous materials [25] has been widely studied using ordered PAAO films.

In most investigations on the anodizing of aluminum, PAAO films are formed in acidic electrolytes, such as sulfuric acid, oxalic acid, phosphoric acid, and etidronic acid [26-33]. At the same time, the PAAO film can also be fabricated via anodizing in alkaline solutions because aluminum oxide dissolves in both acidic and alkaline solutions. Therefore, several research groups have reported the formation behavior of PAAO structures obtained by anodizing in alkaline solutions, particularly using alkaline borate solutions [34-37]. Recently, we found that a self-ordered PAAO film with an interpore distance of 260–590 nm can be fabricated by anodizing in an alkaline sodium tetraborate solution (pH = 8.8–9.1) [38]. The resulting porous alumina possessing a nanoscale spike structure on the pore walls was grown under a novel anodizing regime with a proportionality constant of 3.0 nmV^{-1} for the linear relation of interpore distance–ordering voltage. We also reported that anodizing aluminum in an alkaline sodium metaborate solution (pH = 11.9) caused the formation of a unique PAAO film with an ultra-flat barrier layer and an extremely high porosity (>90%) [39]. Moreover, Nishio et al. recently reported that a characteristic PAAO film with a flat bottom barrier layer and fine porous layer grew during anodizing in a near-neutral potassium oxalate solution (pH = 7.6) [40], even though anodizing in neutral solutions typically causes the formation of a barrier anodic aluminum oxide (BAAO) film. Based on these investigations, anodizing aluminum using electrolyte solutions over a wide pH range has the potential for the fabrication of unconventional PAAO films.

In the present study, we described the morphological changes in a PAAO film fabricated by anodizing aluminum in phosphoric acid and six types of phosphate solutions with a wide pH range from acidic to alkaline. Electron microscopy revealed that the

nanostructure of the anodic oxide changed considerably with the pH of the phosphate solution used in anodizing.

2. Experimental

A high-purity aluminum plate (purity: 5N, thickness: 500 μm, Nippon Light Metal) was used as the starting material for anodizing. The aluminum plate was cut into 20 mm × 10 mm pieces with an electric contact handle. The aluminum pieces were ultrasonically cleaned in 99.5 wt% ethanol for 10 min and electropolished in a mixed solution of 78 vol% acetic acid/22 vol% perchloric acid (70 wt%) at a constant voltage of 28 V and below 280 K for 2 min with a large aluminum sheet used as the cathode.

The electropolished aluminum pieces were potentiostatically anodized in phosphoric acid (H_3PO_4) and the following six phosphate solutions: a) sodium dihydrogen phosphate (NaH_2PO_4), b) sodium hexametaphosphate ($(NaPO_3)_6$), c) sodium tripolyphosphate ($Na_5P_3O_{10}$), d) disodium hydrogen phosphate (Na_2HPO_4), e) sodium diphosphate ($Na_4P_2O_7$), and f) trisodium phosphate (Na_3PO_4). These phosphate solutions possess a wide pH range from acidic to alkaline, and their pH values at each operating temperature are summarized in Table 1. The concentrations of the electrolyte solutions were adjusted to 0.3 M, whereas only $Na_4P_2O_7$ solution was used at 0.2 M because of its low solubility in water at lower temperatures. A platinum plate was employed as the cathode, and the temperature of the electrolyte solution was maintained using a constant-temperature water bath and magnetic stirrer. During potentiostatic anodizing, the voltage was linearly increased to each target voltage for up to the initial 2.5 min, and then the steady-state potentiostatic anodizing process was performed for 60 min using a direct current power supply. The current density measured during the anodizing was recorded using a digital multimeter.

The morphologies of the anodized aluminum specimens were observed using scanning electron microscopy (SEM). Before the SEM observations, the specimens were mounted on a sample holder using carbon tape, and their surface was covered with an electroconductive platinum layer by sputter coating. The vertical cross-sections of the anodized specimens were examined using scanning transmission electron microscopy (STEM). Ultrathin sectioning specimens (25 nm) were prepared using an ultramicrotome and a diamond knife; the specimens were then mounted on a copper mesh grid for STEM observations.

3. Results

3.1 Anodizing aluminum in H_3PO_4

The electropolished aluminum pieces were potentiostatically anodized in 0.3 M H_3PO_4 at 293 K (pH = 1.1), 323 K (pH = 1.4), and 343 K (pH = 1.5). Fig. 1a shows the current–time curves during anodizing at various applied voltages of 20–200 V and temperatures of 293–343 K. At 293 K, the steady-state current density measured after the initial transient stage gradually increased with the applied voltage: from approximately 8

Am^{-2} at 20 V to 80–90 Am^{-2} at 150 V. However, excess anodizing at the highest voltage (200 V) caused a sudden increase in voltage at the initial stage and subsequent non-uniform oxide formation (burning). As the temperature of the H_3PO_4 solution increased to 323 K, the steady-state current density at the same applied voltage increased: from 8 to 93 Am^{-2} at 20 V and from 12 to 142 Am^{-2} at 50 V. Therefore, the growth rate of the anodic oxide increased with increasing solution temperature under the same applied voltage. In addition, with the increase in solution temperature from 293 to 323 K, the burning voltage decreased from 200 to 150 V. These tendencies in electrochemical behavior were also observed at a higher temperature (343 K).

Fig. 1b shows the SEM images of the cross-section of the anodic oxide obtained by anodizing, as shown in Fig. 1a. A typical PAAO film with vertical nanopores and a bottom hemispherical barrier layer was formed at 293 K and 20 V. The diameter of the pores and the width of the pore walls increased as the applied voltage increased to 100 V because the interpore distance of typical PAAO films linearly increases with the applied voltage. The regularity of pore arrangement was not significantly higher in these anodizing cases because the self-ordering voltage during anodizing in H_3PO_4 was approximately 160–195 V [41]. Although similar PAAO films were obtained by anodizing at a higher temperature (343 K), there were many pore-branching structures in the PAAO film because of the higher dissolution environment in H_3PO_4 at high temperature. Based on these experimental results, typical PAAO films with KHR structures were formed by anodizing in H_3PO_4. The morphology of the PAAO film obtained via aluminum anodizing in various phosphate solutions is analyzed below with reference to that formed in H_3PO_4.

3.2 Anodizing aluminum in NaH_2PO_4

The aluminum pieces were potentiostatically anodized in a weakly acidic solution of 0.3 M NaH_2PO_4 at 293 K (pH = 4.3), 323 K (pH = 4.4), and 343 K (pH = 4.5). The steady-state current density slightly increased with the applied voltage at the lower temperature of 293 K. However, these current densities (approximately 0.8–2.5 Am^{-2} at 20–150 V) were much lower than those obtained in H_3PO_4 (Fig. 1a). Similar to that in H_3PO_4, anodizing at 200 V in NaH_2PO_4 resulted in oxide burning. The current densities slightly increased with the temperature of the NaH_2PO_4 solution, whereas the maximum steady-state current density remained small (approximately 10 Am^{-2}). This may be attributed to the low solubility of aluminum oxide in NaH_2PO_4 solution with a higher pH value. Therefore, the growth rate of the anodic oxide formed in the NaH_2PO_4 solution was expected to be considerably lower than that in the H_3PO_4 solution. The burning voltage decreased with increasing solution temperature, similar to that in the H_3PO_4 solution.

Fig. 2b shows SEM images of the cross-section of the anodic oxide formed by anodizing at 100 V and different temperatures (293 and 323 K). Although the anodic oxide formed at 293 K and 100 V was thinner than that obtained in H_3PO_4 because of lower current density during anodizing, a clear PAAO film with nanoscale pores and a

bottom hemispherical barrier layer was observed. Because the current density slightly increased with the temperature of the NaH_2PO_4 solution, relatively thick PAAO films were obtained at 323 K. Therefore, a typical PAAO film was fabricated by anodizing in a weakly acidic NaH_2PO_4 solution, although the current density and corresponding growth rate of the PAAO film were lower than those in H_3PO_4.

3.3 Anodizing aluminum in $(NaPO_3)_6$

The 0.3 M $(NaPO_3)_6$ solution, showing pH = 5.3 at 293 K, 5.5 at 323 K, and 5.5 at 343 K, is less acidic than the NaH_2PO_4 solution of the same concentration. When the aluminum pieces were anodized in this near-neutral solution at different temperatures (293–343 K), extremely low current densities of approximately 0.02–0.1 Am^{-2} at 293 K, 0.2–1.0 Am^{-2} at 323 K, and 0.9–2.0 Am^{-2} at 343 K were obtained during steady-state anodizing (Fig. 3a). This was attributed to the extremely low solubility of aluminum oxide in the $(NaPO_3)_6$ solution. There were no significant changes in the shape of the current–time curve as the applied voltage increased, whereas anodizing at 200 V caused a sudden voltage increase and oxide burning at each temperature.

Fig. 3b shows SEM images of the cross-section of the anodic oxide formed at 100 V at three different temperatures. A uniform anodic oxide film with a flat interface between the anodic oxide and aluminum substrate was obtained at 293 K, although an extremely small unevenness could be observed on the surface. Because this unevenness may have been caused by the electroconductive platinum layer deposited before the SEM observation, this anodic oxide was also observed by high-angle annular dark field (HAADF)-STEM and TEM without the deposition of the electroconductive layer (Fig. 3c). The HAADF-STEM image and the corresponding high-resolution TEM image show that the surface of the anodic oxide was perfectly flat without any pores. Thus, a BAAO film formed in a $(NaPO_3)_6$ solution at low temperature. However, a clear uneven structure was formed on the surface as the temperature increased to 323 K, and the size of the unevenness significantly increased as the temperature further increased to 343 K. Notably, a slightly curved shape was observed at the interface between the anodic oxide and the aluminum substrate, which was similar in shape to the bottom of typical PAAO films. Because the solubility of aluminum oxide at 323 and 343 K is higher than at 293 K, a porous layer may have formed at these higher temperatures because of the slight dissolution of aluminum oxide on the surface. Based on these observations, a uniform BAAO film was formed in a $(NaPO_3)_6$ solution at lower temperatures, whereas a PAAO film with an extremely thin porous layer was obtained at higher temperatures.

3.4 Anodizing aluminum in $Na_5P_3O_{10}$

0.3 M $Na_5P_3O_{10}$ solution is a weak alkaline solution with a pH of 8.7 at 293 K, 8.7 at 323 K, and 8.6 at 343 K. During anodizing in 0.3 M $Na_5P_3O_{10}$ at 293 K (Fig. 4a), extremely low steady-state current densities of approximately 0.2–0.5 Am^{-2} were obtained in the entire range of applied voltages (20–150 V). This electrochemical

behavior is very similar to that observed in $(NaPO_3)_6$ solution (Fig. 3a). However, the current density gradually increased with the temperature of the $Na_5P_3O_{10}$ solution, from the effect not observed with the $(NaPO_3)_6$ solution, and relatively higher current densities of approximately 60–80 Am^{-2} were obtained at 343 K. The current densities measured at lower voltages of 20–100 V increased with anodizing time, whereas those measured at 150 V were almost unchanged during anodizing without the initial stage. A higher applied voltage of 200 V resulted in oxide burning at all temperatures.

Fig. 4b shows SEM images of the cross-section of the anodic oxide formed at 100 V and three different temperatures. A uniform anodic oxide film was observed in the SEM image obtained by anodizing at a lower temperature (293 K). However, when this specimen was observed using high-magnification HAADF-STEM, extremely narrow pores measuring approximately 20 nm in length were clearly observed on the entire surface of the anodic oxide (Fig. 4c). Interestingly, the morphology of the anodic oxide drastically changed as the temperature increased to 323 K: a thick PAAO film with tens of nanometer-scale bumps on the entire pore walls appeared because of higher current density. This "feathering" of pore walls grown in the PAAO film has been reported during anodizing in chromic acid and sodium tetraborate solutions [38,42,43]. A similar PAAO film with bumpy pore morphology was observed at a higher temperature (343 K). As a result of anodizing in weakly alkaline $Na_5P_3O_{10}$ solution, a thin PAAO film with an outer narrow porous layer and an inner flat barrier layer was formed at lower temperatures, whereas a thick PAAO film with bumpy pore walls and a bottom hemispherical barrier layer was obtained at higher temperatures.

3.5 Anodizing aluminum in Na_2HPO_4

0.3 M Na_2HPO_4 is also a weak alkaline solution with pH of 9.0 at 293 K, 8.8 at 323 K, and 8.6 at 343 K; these pH values are very similar to those of the 0.3 M $Na_5P_3O_{10}$. However, the morphology of the PAAO film formed in Na_2HPO_4 at higher temperatures was significantly different from that obtained in $Na_5P_3O_{10}$. Fig. 5a shows the current density–time curves obtained during potentiostatic anodizing in 0.3 M Na_2HPO_4 solution at 393–343 K. The current densities during steady-state anodizing at 293 K exhibited extremely low values (below 2.0 Am^{-2}), whereas oxide burning occurred at 200 V. The current density increased with the temperature of the Na_2HPO_4 solution: 4.0–5.0 Am^{-2} at 323 K and 15.0–40.0 Am^{-2} at 343 K. The current density was independent of the applied voltage, and similar current–voltage curves were obtained at the same temperature. The burning voltage decreased from 200 to 150 V as the solution temperature increased.

The anodic oxide obtained at 100 V and different temperatures (293–343 K) was examined using SEM (Fig. 5b). A relatively uniform anodic oxide film was observed on the aluminum surface at 293 K. Similar to the case with $Na_5P_3O_{10}$ solution, a narrow porous layer of approximately 25 nm in thickness was observed on the flat BAAO film via HAADF-STEM (Fig. 5c). The thickness of this narrow porous layer increased with the temperature of the Na_2HPO_4 solution, although the morphology of the bottom BAAO

layer remained unchanged. The top layer of the anodic oxide dissolved at the higher temperature (343 K) owing to its high solubility in the anodizing environment, and a pyramidal structure consisting of many alumina nanofibers was formed on the surface. Typically, the interpore distance of the PAAO film increases with increasing applied voltage, and the following relationship is observed [38]:

$$D_{int} = 2.5\ U_a \qquad (1)$$

where D_{int} corresponds to the interpore distance (nm), and U_a is the applied voltage (V). Although the interpore distance of the PAAO film formed at 100 V was calculated to be 250 nm, this value is clearly inconsistent with that obtained by anodizing in Na_2HPO_4. The nanostructure of the PAAO film formed by anodizing in Na_2HPO_4 was significantly different from the typical KHR-model PAAO film in terms of the interpore distance and the morphology of the bottom barrier layer.

3.6 Anodizing aluminum in $Na_4P_2O_7$

Aluminum pieces were potentiostatically anodized in an alkaline 0.2 M $Na_4P_2O_7$ at 293 K (pH = 10.5), 323 K (pH = 9.9), and 343 K (pH = 9.6); these pH values are slightly higher than those of $Na_5P_3O_{10}$ and Na_2HPO_4 solutions. At the lower temperature (293 K), the current densities were low (approximately 1.5–4.0 Am^{-2}). The current density increased considerably with the temperature of the Na_2HPO_4 solution: from approximately 50 Am^{-2} at 323 K to 175–250 Am^{-2} at 343 K. At the same temperature, the current density was almost independent of the applied voltage.

Fig. 6b shows SEM images of the cross-section of the anodic oxide formed at 100 V and three different temperatures. A PAAO film consisting of an outer porous layer and inner flat barrier layer was formed at a low temperature (293 K). As the temperature of the Na_2HPO_4 solution increased to 323 and 343 K, PAAO films consisting of an outer porous layer with feathering pore walls and an inner hemispherical barrier layer were observed. The nanomorphologies of the PAAO film were similar to those obtained in the $Na_5P_3O_{10}$ solution, although the thickness of porous layer formed at 293 K was thicker than that formed in $Na_5P_3O_{10}$ due to the higher current density.

3.7 Anodizing aluminum in Na_3PO_4

0.3 M Na_3PO_4 has the highest pH of the seven electrolytes used in the present study: pH = 12.5 at 293 K, 11.7 at 323 K, and 10.9 at 343 K. During anodizing in the Na_3PO_4 solution at 293 K (Fig. 7a), the steady-state current density was much higher than in previous acidic and alkaline solutions (250–600 Am^{-2}). As the temperature of the Na_3PO_4 solution increased to 323–343 K, the current density exceeded 1000 Am^{-2}. At the same time, the burning voltage decreased with the increase in solution temperature from 150 V at 293 K to 50 V at 343 K; thus, anodizing at higher applied voltage could not be achieved at high temperatures.

Fig. 7b shows the SEM images of the cross-section of the anodic oxide formed at 50–100 V and 293 K. As shown in Fig. 7b, a typical PAAO film consisting of an outer

high-aspect-ratio porous layer and inner hemispherical barrier layer was obtained at 50 V. However, an unconventional PAAO film with a flat bottom barrier layer, which was observed in Na_2HPO_4 and $Na_4P_2O_7$ solutions, was obtained at 100 V. The porous layer was significantly thicker than those obtained in those solutions owing to the high current density during anodizing.

4. Discussion

4.1 Effect of the pH value on the current density during anodizing

The current density measured during anodizing, which corresponds to the growth rate of the anodic oxide, was significantly different for each electrolyte (phosphoric acid and six phosphates). Fig. 8 summarizes the effect of the pH of the electrolyte on the current density during anodizing for 62.5 min at 100 V (shown in Figs. 1–7). At the lower temperature (293 K), the current density exhibited much higher values of approximately 10^1–10^2 Am^{-2} in H_3PO_4 (pH = 1.1) and Na_3PO_4 solutions (pH = 12.5). As the pH was shifted closer to the neutral region, current density rapidly decreased, with 10^{-2}–10^{-1} Am^{-2} obtained in $(NaPO_3)_6$ (pH = 5.3), $Na_5P_3O_{10}$ (pH = 8.7), and Na_2HPO_4 solutions (pH = 9.0). Similar behaviors were observed at higher temperatures (323 and 343 K). The dissolution rate of aluminum oxide strongly depends on the pH of the electrolyte solution and increases exponentially as the pH shifts in the acidic or alkaline directions [44]. Because a BAAO film was formed by potentiostatic anodizing in an environment where aluminum oxide is almost insoluble, an extremely low current density was measured after the formation of the BAAO film. Conversely, higher current density was continuously measured in electrolyte solutions with lower and higher pH values because of the continuous anodic oxide formation in the environment where it has higher solubility. Therefore, the V-shaped current density–pH relation was obtained, as shown in Fig. 8.

4.2 Effect of the anodizing condition on the morphology of anodic oxide

As shown in Figs. 1–7, the morphology of the anodic oxide was drastically changed by anodizing in different phosphate solutions. Fig. 9 shows the schematic models of the anodic oxide morphologies obtained in different pH ranges. In addition, the morphologies of the anodic oxide obtained in six phosphate solutions at 100 V were summarized in Table 2. Anodizing aluminum in acidic H_3PO_4 causes the formation of a PAAO film with smooth pore walls and a hemispherical barrier layer (A-type PAAO, Figs. 1 and 9). A similar PAAO film was obtained in acidic NaH_2PO_4 (Fig. 2). Such PAAO films are well-known as KHR structures that can be obtained via anodizing in acidic electrolyte solutions. In the $(NaPO_3)_6$ solution with a near-neutral pH value, a complete BAAO film was formed at a lower temperature (Fig. 3). However, the top surface of the BAAO film slightly dissolved at higher temperatures owing to its higher solubility, a narrow porous layer was formed on the surface, and a wavy barrier layer was formed at the bottom of the anodic oxide. This structure is similar to the A-type PAAO film.

In alkaline phosphate solutions, two types of characteristic PAAO films were

formed. One of them was a PAAO film consisting of an outer porous layer with feathered pore walls and an inner hemispherical barrier layer (C-type PAAO, Fig. 9). This C-type PAAO film was formed by anodizing at higher temperature in $Na_5P_3O_{10}$ (Fig. 4) and $Na_4P_2O_7$ (Fig. 6). The second morphology was a PAAO film consisting of an outer porous layer with elongated pores and an inner flat barrier layer (D-type PAAO, Fig. 9). Hebert and Thompson reported that the hemispherical barrier layer at the bottom of the PAAO film is formed because of the compressive stress and subsequent oxide flow during anodizing [45-49].This D-type PAAO film was typically obtained by anodizing at lower temperature in alkaline $Na_5P_3O_{10}$ (Fig. 4), Na_2HPO_4 (Fig. 5), $Na_4P_2O_7$ (Fig. 6), and Na_3PO_4 (Fig. 7). Namely, the morphology of anodic oxide varies greatly depending on the type of electrolyte used and operating conditions during anodizing aluminum in alkaline solutions.

The formation of characteristic C-type and D-type PAAO films has been previously reported by anodizing in alkaline sodium tetraborate [38] and sodium metaborate [39] solutions. Therefore, there is no doubt that the pH value of the electrolyte solution strongly affects the nanomorphology of PAAO film. It is widely accepted that for the growth of anodic alumina both Al^{+3} and oxygen-containing anions, such as O^{2-} or OH^-, are mobile in the oxide under high electric field [10]. The difference between O^{2-} and OH^- during migration by anodizing in acidic and alkaline solutions may cause the nanostructural changes in the PAAO film. On the other hand, the feathering of pore walls can also be obtained by anodizing in chromic acid, although anodizing in other acidic electrolyte solutions causes the formation of smooth pore walls. Thompson et al. reported that the addition of sulfate to chromic acid caused an increase in the sulfur content of the anodic oxide and decreased feathering of the pore walls [50]. Anodizing in sulfuric acid leads to the formation of smooth pore walls; thus, smoothing in chromic acid containing sulfate was caused by sulfate. The reason for the formation of feathering on pore walls during anodizing in several alkaline phosphates and chromic acid is still unknown; thus further nanostructural characterizations during anodizing under various operating conditions are required.

Pashchanka et al. reported the electro-convective model for the origin of self-organization of PAAO film during anodizing [41]. This model is based on the Rayleigh–Bénard convection currents near aluminum without the field-assisted dissolution of pre-formed anodic alumina, and allows the formation of a typical PAAO film consisting of an outer porous layer, an inner hemispherical barrier layer, and the corresponding hemispherical aluminum dimples. However, a PAAO film consisting of an outer porous layer and an inner flat barrier layer was formed in some cases of anodizing in alkaline phosphate solutions, and the interface between the anodic oxide and aluminum substrate exhibited an extremely flat without hexagonal nanostructure. Therefore, the formation of this unique PAAO film with the flat barrier layer may be caused by the field-assisted dissolution model rather than by the Rayleigh–Bénard convection model. Note that such a characteristic PAAO film, which is different from the typical PAAO film, is not formed

by anodizing in acidic solutions, and is obtained by anodizing in neutral and alkaline solutions. On the other hand, the formation of typical hemispherical barrier layer may be explained by the electro-convective model and flow model. The pH value and temperature of the electrolyte solution has a significant effect on the nanomorphology of the barrier layer.

The anion incorporation into the anodic oxide during anodizing may affect the important properties of anodic oxide films, such as hardness and corrosion resistance [51]. Thus, it is important to understand the presence or absence of incorporated anions in the anodic oxide. Supplementary Figure 1 shows the GD-OES depth profiles of the specimen anodized in NaH_2PO_4, $(NaPO_3)_6$, $Na_5P_3O_{10}$, Na_2HPO_4, and $Na_4P_2O_7$ at 100 V for 62.5 min. Phosphorus, which resulted from the incorporated anions originating from the electrolyte solution, was distributed in the A-type PAAO, D-type PAAO, and BAAO films. In addition, it is widely known that the PAAO film formed by anodizing in H_3PO_4 (i.e., A-type PAAO) also contains incorporated anions [10]. On the other hand, the C-type PAAO film, which is formed in $Na_5P_3O_{10}$ and $Na_4P_2O_7$ solutions, consisted of anion-free aluminum oxide. Therefore, there are differences in the presence or absence of anions depending on the electrolyte, even if the similar phosphate anions are used during anodizing aluminum.

The ratio of the thickness of the porous layer and barrier layer (PL/BL) and the pore size of the PAAO film formed by each anodizing were measured. Fig. 10 summarizes the effect of the current density on the a) PL/BL value and b) pore size obtained by anodizing for 62.5 min at 100 V. The PL/BL value increased with the current density (Fig. 10a), because the current density after the initial anodizing period is closely related to the amount of porous film growth. However, there was no clear, linear relation between the pore size and current density (Fig. 10b). Although the pore size increased with the current density in many cases, several pores remained approximately 10-20 nm at higher current densities in alkaline solutions with relatively higher pH values. In these cases, narrow PAAO films with a bottom flat barrier layer were typically formed on the aluminum surface (D-type PAAO).

5. Conclusions

Phosphoric acid and six phosphate solutions with a wide pH range from acidic to alkaline were used as the electrolyte solutions for anodizing aluminum. Morphological characterization of the obtained oxide layer was conducted using SEM and STEM. The following conclusions were drawn from our investigation.

1) High current density (more than 10^2 Am^{-2}) was observed during anodizing at lower or higher pH values, and it rapidly decreased to 10^{-2}–10^{-1} Am^{-2} as the pH was shifted closer to the neutral region.

2) A typical PAAO film consisting of an outer porous layer and an inner hemispherical barrier layer, which is based on the KHR model, was formed in acidic H_3PO_4 and NaH_2PO_4.

3) A uniform BAAO film or PAAO film with a narrow porous layer was formed in near-neutral $(NaPO_3)_6$ because of the low solubility of aluminum oxide.
4) Two types of PAAO films were formed in alkaline $Na_5P_3O_{10}$, Na_2HPO_4, $Na_4P_2O_7$, and Na_3PO_4: PAAO film consisting of an outer porous layer with feathered pore walls and an inner hemispherical barrier layer, and PAAO film consisting of an outer porous layer with elongated pores and an inner flat barrier layer. Therefore, the nanomorphology of the PAAO film formed in alkaline solutions was different from that obtained in typical acidic solutions.

Acknowledgments

This study was financially supported by the Japan Society for the Promotion of Science (JSPS) KAKENHI (grant numbers: 19H02470 and 22H01824) and the Nanotechnology Platform Program (grant number: A-21-HK-0001) of the Ministry of Education, Culture, Sports, Science and Technology (MEXT), Japan. The authors thank Mr. Ryo Oota in the high-voltage electron microscope laboratory and the technical staff in the laboratory of nano-micro material analysis for STEM and SEM observations.

References

1) G.E. Thompson, G.C. Wood, Porous anodic film formation on aluminium, Nature 290 (1981) 230-232, https://doi.org/10.1038/290230a0.
2) S. Ono, Nanostructure Analysis of Anodic Films Formed on Aluminum-Focusing on the Effects of Electric Field Strength and Electrolyte Anions, Molecules, 26 (2021) 7270, https://doi.org/10.3390/molecules26237270.
3) K.S. Choudhari, C.H. Choi, S. Chidangil, S.D. George, Recent Progress in the Fabrication and Optical Properties of Nanoporous Anodic Alumina, Nanomaterials, 12 (2022) 444, https://doi.org/10.3390/nano12030444.
4) Z. Zhao, Y. Liu, L. Yuan, The Variation of Anodization Conditions and the Structural Properties of Nanoporous Anodic Alumina (NAA) within Different Acidic Solutions, J. Electrochem. Soc. 169 (2022) 043503, https://orcid.org/0000-0003-1890-5177.
5) S.Z. Chu, K. Wada, S. Inoue, M. Isogai, Y. Katsuta, A. Yasumori, Large-scale fabrication of ordered nanoporous alumina films with arbitrary pore intervals by critical-potential anodization, J. Electrochem. Soc. 153 (2006) B384-B391, https://doi.org/10.1149/1.2218822.
6) F. Keller, M.S. Hunter, D.L. Robinson, Structural features of oxide coatings on aluminum, J. Electrochem. Soc. 100 (1953) 411-419, https://doi.org/10.1149/1.2781142.
7) H., Masuda, K. Fukuda, Ordered metal nanohole arrays made by a two-step replication of honeycomb structures of anodic alumina, Science 268 (1995) 1466-1468, https://doi.org/10.1126/science.268.5216.1466.

8) H. Masuda, F. Hasegwa, S. Ono, Self-ordering of cell arrangement of anodic porous alumina formed in sulfuric acid solution, J. Electrochem. Soc. 144 (1997) L127-L130, https://doi.org/10.1149/1.1837634.
9) H. Masuda, K. Yada, A. Osaka, Self-ordering of cell configuration of anodic porous alumina with large-size pores in phosphoric acid solution, Jpn. J. Appl. Phys. 37 (1998) L1340-L1342, https://doi.org/10.1143/JJAP.37.L1340.
10) W. Lee, S.J. Park, Porous anodic aluminum oxide: anodization and templated synthesis of functional nanostructures, Chem. Rev. 114 (2014) 7487-7556, https://doi.org/10.1021/cr500002z.
11) T. Kikuchi, D. Nakajima, O. Nishinaga, S. Natsui, R.O. Suzuki, Porous aluminum oxide formed by anodizing in various electrolyte species, Curr. Nanosci. 11 (2015) 560-571, https://doi.org/10.2174/1573413711999150608144742.
12) A. Santos, Nanoporous anodic alumina photonic crystals: Fundamentals, developments and perspectives, J. Mater. Chem. C 5 (2017) 5581-5599, https://doi.org/10.1039/C6TC05555A.
13) A. Ruiz-Clavijo, O. Caballero-Calero, M. Martin-Gonzalez, Revisiting anodic alumina templates: From fabrication to applications, Nanoscale 13 (2021) 2227-2265, https://doi.org/10.1039/D0NR07582E.
14) T. Yanagishita, R. Fujimura, K. Nishio, H. Masuda, Preparation of uniform-sized polymer nanofibers by extrusive spinning using ordered anodic porous alumina, Chem. Lett. 39 (2010) 188-189, https://doi.org/10.1246/cl.2010.188.
15) T. Kondo, N. Kitagishi, T. Fukushima, T. Yanagishita, H. Masuda, Fabrication of aluminum nanowires by mechanical deformation of Al using anodic porous alumina molds, Mater. Express 6 (2016) 363-366, https://doi.org/10.1166/mex.2016.1316.
16) T. Yanagishita, H. Takai, T. Kondo, H. Masuda, SnO_2 nanofibers prepared by wet spinning using an ordered porous alumina spinneret, Nanotechnology 32 (2021) 145603, https://orcid.org/0000-0002-6079-9294.
17) T. Kondo, M. Tanji, K. Nishio, H. Masuda, Cross-striped ordered arrays of Au nanoparticles in anodic porous alumina matrix, Electrochem. Solid-state Lett. 9 (2006) C189-C191, https://doi.org/10.1149/1.2351959.
18) T. Kondo, H. Masuda, K. Nishio, SERS in ordered array of geometrically controlled nanodots obtained using anodic porous alumina, J. Phys. Chem. C 117 (2013) 2531-2534, https://doi.org/10.1021/jp306470r.
19) H. Masuda, M. Ohya, H. Asoh, M. Nakao, M. Nohtomi, T. Tamamura, Photonic crystal using anodic porous alumina, Jpn. J. Appl. Phys. 38 (1999) L1403-L1405, https://doi.org/10.1143/JJAP.38.L1403.
20) H. Masuda, M. Yamada, F. Matsumoto, S. Yokoyama, S. Mashiko, M. Nakao, K. Nishio, asing from Two-Dimensional Photonic Crystals Using Anodic Porous Alumina, Adv. Mater. 18 (2006) 213-216, https://doi.org/10.1002/adma.200401940.
21) W. Lee, H. Han, A. Lotnyk, M.A Schubert, S. Senz, M. Alexe, D. Hesse, S. Baik, U. Gösele, Individually addressable epitaxial ferroelectric nanocapacitor arrays with near

Tb inch^{-2} density, Nat. Nanotechnol. 3 (2008) 402-407, https://doi.org/10.1038/nnano.2008.161
22) A. Takenaga, T. Kikuchi, S. Natsui, R.O. Suzuki, Self-ordered aluminum anodizing in phosphonoacetic acid and its structural coloration, ECS Solid State Lett. 4 (2015) P55-P58, https://doi.org/10.1149/2.0021508ssl.
23) H. Masuda, K. Yasui, K. Nishio, Fabrication of ordered arrays of multiple nanodots using anodic porous alumina as an evaporation mask, Adv. Mater. 12 (2000) 1031-1033, https://doi.org/10.1002/1521-4095(200007)12:14<1031::AID-ADMA1031>3.0.CO2-R.
24) M.S. Sander, L.S. Tan, Nanoparticle arrays on surfaces fabricated using anodic alumina films as templates, Adv. Funct. Mater. 13 (2003) 393-397, https://doi.org/10.1002/adfm.200304290.
25) S.Z. Kure-Chu, K. Osaka, H. Yashiro, H. Segawa, K. Wada, S. Inoue, Controllable fabrication of networked three-dimensional nanoporous anodic alumina films on low-purity Al materials, J. Electrochem. Soc. 162 (2014) C24-C34, https://doi.org/10.1149/2.0511501jes.
26) G.D. Sulka, S. Stroobants, V. Moshchalkov, G. Borghs, J.P. Celis, Synthesis of well-ordered nanopores by anodizing aluminum foils in sulfuric acid, J. Electrochem. Soc. 149 (2002) D97-D103, https://doi.org/10.1149/1.1481527.
27) I.D. Graeve, H. Terryn, G.E. Thompson, Influence of local heat development on film thickness for anodizing aluminum in sulfuric acid, J. Electrochem. Soc. 150 (2003) B158-B165, https://doi.org/10.1149/1.1560639.
28) A.P. Leontiev, I.V. Roslyakov, K.S. Napolskii, Complex influence of temperature on oxalic acid anodizing of aluminium, Electrochim. Acta 319 (2019) 88-94, https://doi.org/10.1016/j.electacta.2019.06.111.
29) H. Asoh, T. Sano, Forming Hard Anodic Films on Aluminum by Anodization in Oxalic Acid and Alcohol, J. Electrochem. Soc. 168 (2021) 103506, https://doi.org/10.1149/1945-7111/ac2ec1.
30) K. Surawathanawises, X. Cheng, Nanoporous anodic aluminum oxide with a long-range order and tunable cell sizes by phosphoric acid anodization on pre-patterned substrates, Electrochim. Acta 117 (2014) 498-503, https://doi.org/10.1016/j.electacta.2013.11.144.
31) A. Gasco-Owens, D. Veys-Renaux, V. Cartigny, E. Rocca, Large-pores anodizing of 5657 aluminum alloy in phosphoric acid: an in-situ electrochemical study, Electrochim. Acta 382 (2021) 138303, https://doi.org/10.1016/j.electacta.2021.138303.
32) T. Kikuchi, O. Nishinaga, S. Natsui, R. O. Suzuki, Fabrication of self-ordered porous alumina via etidronic acid anodizing and structural color generation from submicrometer-scale dimple array, Electrochim. Acta 156 (2015) 235-243, https://doi.org/10.1016/j.electacta.2014.12.171.

33) T. Kikuchi, O. Nishinaga, S. Natsui, R. O. Suzuki, Self-ordering behavior of anodic porous alumina via selenic acid anodizing, Electrochim. Acta 137 (2014) 728-735, https://doi.org/10.1016/j.electacta.2014.06.078.
34) S. John, V. Balasubramanian, B.A. Shenoi, Studies on anodizing of aluminium in alkaline electrolyte using alternating current, Surf. Technol. 26 (1985) 207-216, https://doi.org/10.1016/0376-4583(85)90117-7.
35) A. Pakes, G.E. Tompson, P. Skeldon, P.C. Morgan, K. Shimizu, Anodizing of Aluminium in Borax Solution, Trans. IMF 77 (1999) 171-177, https://doi.org/10.1080/00202967.1999.11871276.
36) S.J. Garcia-Vergara, P. Skeldon, G.E., Thompson, H. Habazaki, Formation of porous anodic alumina in alkaline borate electrolyte, Thin Solid Films 515 (2007) 5418-5423, https://doi.org/10.1016/j.tsf.2007.01.013.
37) T. Kikuchi, K. Kunimoto, H. Ikeda, D. Nakajima, R.O. Suzuki, S. Natsui, Fabrication of anodic porous alumina via galvanostatic anodizing in alkaline sodium tetraborate solution and their morphology, J. Electroanal. Chem. 846 (2019) 113152, https://doi.org/10.1016/j.jelechem.2019.05.034.
38) M. Iwai, T. Kikuchi, R.O. Suzuki, Self-ordered nanospike porous alumina fabricated under a new regime by an anodizing process in alkaline media, Sci. Rep. 11 (2021) 7240, https://doi.org/10.1038/s41598-021-86696-z.
39) M. Iwai, T. Kikuchi, Fabrication of unique porous alumina films with extremely high porosity and an ultra-flat barrier layer by anodizing aluminum in sodium metaborate, Electrochim. Acta 399 (2021) 139440, https://doi.org/10.1016/j.electacta.2021.139440.
40) K. Nishio, R. Sasaki, Anodization of Al in Neutral Oxalate Solution to Form Unusually Fine Nanoporous Film, Chem. Lett. 48 (2019) 1126-1129, https://doi.org/10.1246/cl.190446.
41) M. Pashchanka, J.J. Schneider, Origin of self-organisation in porous anodic alumina films derived from analogy with Rayleigh–Bénard convection cells, 21 (2011) 18761-18767, 10.1039/C1JM13898G.
42) S.J. Garcia-Vergara, P. Skeldon, G.E. Thompson, H. Habazaki, A tracer investigation of chromic acid anodizing of aluminium, Surf. Interface Anal. 39 (2007) 860-864, https://doi.org/10.1002/sia.2601.
43) T. Kikuchi, M. Yamashita, M. Iwai, R.O. Suzuki, Self-Ordering of Porous Anodic Alumina Fabricated by Anodizing in Chromic Acid at High Temperature, J. Electrochem. Soc. 168 (2021) 093501, https://doi.org/10.1149/1945-7111/ac2101.
44) C. Vargel, Corrosion of aluminum, 1st edition, Elsevier Science, 2004.
45) J. E. Houser, K. R. Hebert, The role of viscous flow of oxide in the growth of self-ordered porous anodic alumina films, Nat. Mater. 8 (2009) 415-420, https://doi.org/10.1038/nmat2423.
46) Ö.Ö. Çapraz, P. Shrotriya, P. Skeldon, G.E. Thompson, K.R. Hebert, Role of oxide stress in the initial growth of self-organized porous aluminum oxide, Electrochim. Acta 167 (2015) 404-411, https://doi.org/10.1016/j.electacta.2015.03.017.

47) K.R. Hebert, P. Mishra, Model of Stress Generation in Anodic Aluminum Oxide Films: Part I. Origin of Stress at the Film Interfaces, J. Electrochem. Soc. 165 (2018) E737-E743, https://doi.org/10.1149/2.0221814jes.
48) K.R. Hebert, P. Mishra, Model of Stress Generation in Anodic Aluminum Oxide Films: Part II. Surface Stress Accumulation Preceding Formation of Self-Organized Pore Arrays, J. Electrochem. Soc. 165 (2018) E744-E750, https://doi.org/10.1149/2.0231814jes.
49) P. Mishra, K.R. Hebert, Self-organization of anodic aluminum oxide layers by a flow mechanism, Electrochim. Acta 340 (2020) 135879, https://doi.org/10.1016/j.electacta.2020.135879.
50) D. Elabar, A. Němcová, T. Hashimoto, P. Skeldon, G.E. Thompson, Effect of sulphate impurity in chromic acid anodizing of aluminium, Corr. Sci. 100 (2015) 377-385, https://doi.org/10.1016/j.corsci.2015.08.019.
51) Y. Suzuki, K. Kawahara, T. Kikuchi, R. O. Suzuki, S. Natsui, Corrosion-resistant porous alumina formed via anodizing aluminum in etidronic acid and its pore-sealing behavior in boiling water, J. Electrochem. Soc. 166 (2019) C261-C-269, https://doi.org/10.1149/2.0221912jes.

Captions

Table 1 The pH of H_3PO_4 and six phosphate solutions used in this investigation.

Table 2 The nanomorphology of the anodic oxide formed by anodizing in six phosphate solutions.

Figure 1 a) Current density–time curves during anodizing of aluminum in 0.3 M H_3PO_4 at the temperatures of 293, 323, and 343 K and applied voltages of 20–200 V. b) The nanostructures of the anodic oxide obtained after anodizing for 62.5 min under various conditions.

Figure 2 a) Current density–time curves during anodizing of aluminum in 0.3 M NaH_2PO_4 at 293, 323, and 343 K and applied voltages of 20–200 V. b) The nanostructures of the anodic oxide obtained after anodizing for 62.5 min under various conditions.

Figure 3 a) Current density–time curves during anodizing of aluminum in a 0.3 M $(NaPO_3)_6$ at 293, 323, and 343 K and applied voltages of 20–200 V. b) The nanostructures of the anodic oxide obtained after anodizing for 62.5 min under various conditions. c) A HAADF-STEM image and a high-resolution TEM image of the anodic oxide formed at 293 K and 100 V.

Figure 4 a) Current density–time curves during anodizing of aluminum in 0.3 M $Na_5P_3O_{10}$ at 293, 323, and 343 K and applied voltages of 20–200 V. b) The nanostructures of the anodic oxide obtained after anodizing for 62.5 min under various conditions. c) A HAADF-STEM image of the anodic oxide formed at 293 K and 100 V.

Figure 5 a) Current density–time curves during anodizing of aluminum in 0.3 M Na_2HPO_4 at 293, 323, and 343 K and applied voltages of 20–200 V. b) The nanostructures of the anodic oxide obtained after anodizing for 62.5 min under various conditions. c) A HAADF-STEM image of the anodic oxide formed at 293 K and 100 V.

Figure 6 a) Current density–time curves during anodizing of aluminum in 0.2 M Na_2HPO_4 solution at 293, 323, and 343 K and applied voltages of 20–200 V. b) The nanostructures of the anodic oxide obtained after anodizing for 62.5 min under various conditions.

Figure 7 a) Current density–time curves during anodizing of aluminum in 0.3 M Na_3PO_4 at 293, 323, and 343 K and applied voltages of 20–150 V. b) The nanostructures of the anodic oxide obtained after anodizing for 62.5 min under various conditions.

Figure 8 Effect of pH on the current density during anodizing at 100 V for 62.5 min.

Figure 9 Schematics of the anodic oxide formed via aluminum anodizing in various phosphate solutions with different pH values.

Figure 10 Effect of the current density on the a) ratio of the thickness of the porous layer and barrier layer (PL/BL) and b) pore size of the PAAO film obtained by anodizing at 100 V for 62.5 min.

Table 1

Electrolyte solutions	293 K	323 K	343 K
0.3 M phosphoric acid (H_3PO_4)	1.1	1.4	1.5
0.3 M sodium dihydrogen phosphate (NaH_2PO_4)	4.3	4.4	4.5
0.3 M sodium hexametaphosphate ($(NaPO_3)_6$)	5.3	5.5	5.5
0.3 M sodium tripolyphosphate ($Na_5P_3O_{10}$)	8.7	8.7	8.6
0.3 M disodium hydrogen phosphate (Na_2HPO_4)	9.0	8.8	8.6
0.2 M sodium diphosphate ($Na_4P_2O_7$)	10.5	9.9	9.6
0.3 M trisodium phosphate (Na_3PO_4)	12.5	11.7	10.9

Table 2

Electrolytes	Type of oxide	
	Lower temperature	higher temperture
sodium dihydrogen phosphate (NaH_2PO_4)	A-type PAAO	A-type PAAO
sodium hexametaphosphate ($(NaPO_3)_6$)	BAAO	A-type PAAO
sodium tripolyphosphate ($Na_5P_3O_{10}$)	D-type PAAO	C-type PAAO
disodium hydrogen phosphate (Na_2HPO_4)	D-type PAAO	D-type PAAO
sodium diphosphate ($Na_4P_2O_7$)	D-type PAAO	C-type PAAO
trisodium phosphate (Na_3PO_4)	D-type PAAO	-

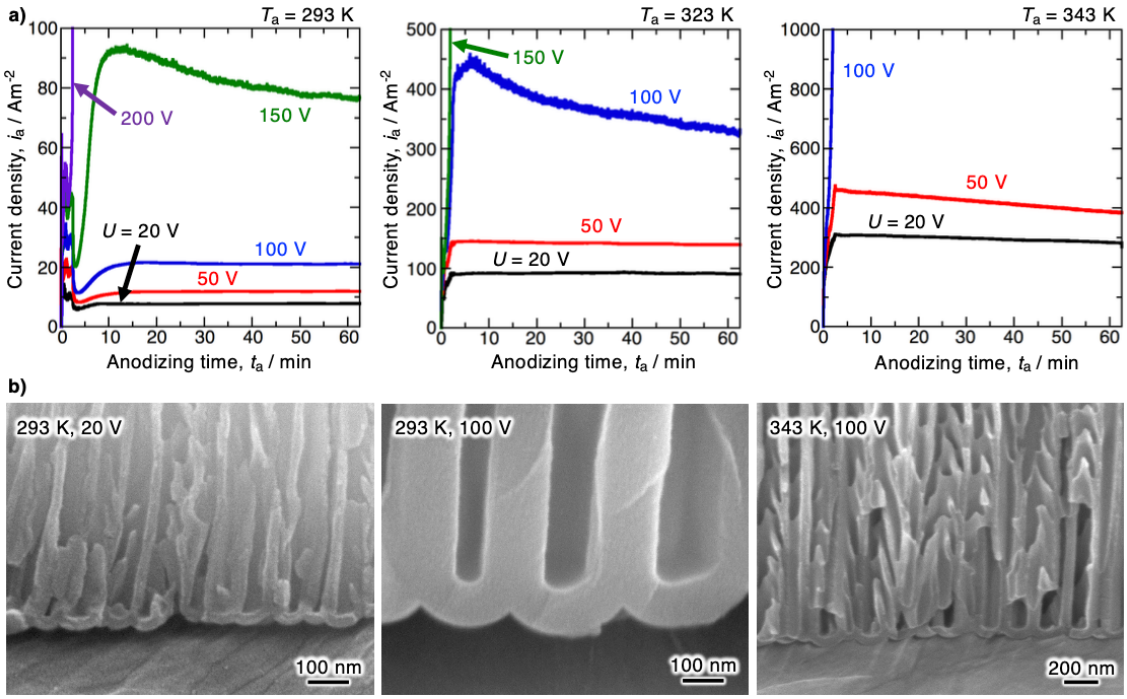
a)
T_a = 293 K
T_a = 323 K
T_a = 343 K
Current density, i_a / Am^{-2}
Anodizing time, t_a / min
200 V
150 V
100 V
50 V
U = 20 V
b)
293 K, 20 V
293 K, 100 V
343 K, 100 V
100 nm
100 nm
200 nm

Figure 1.

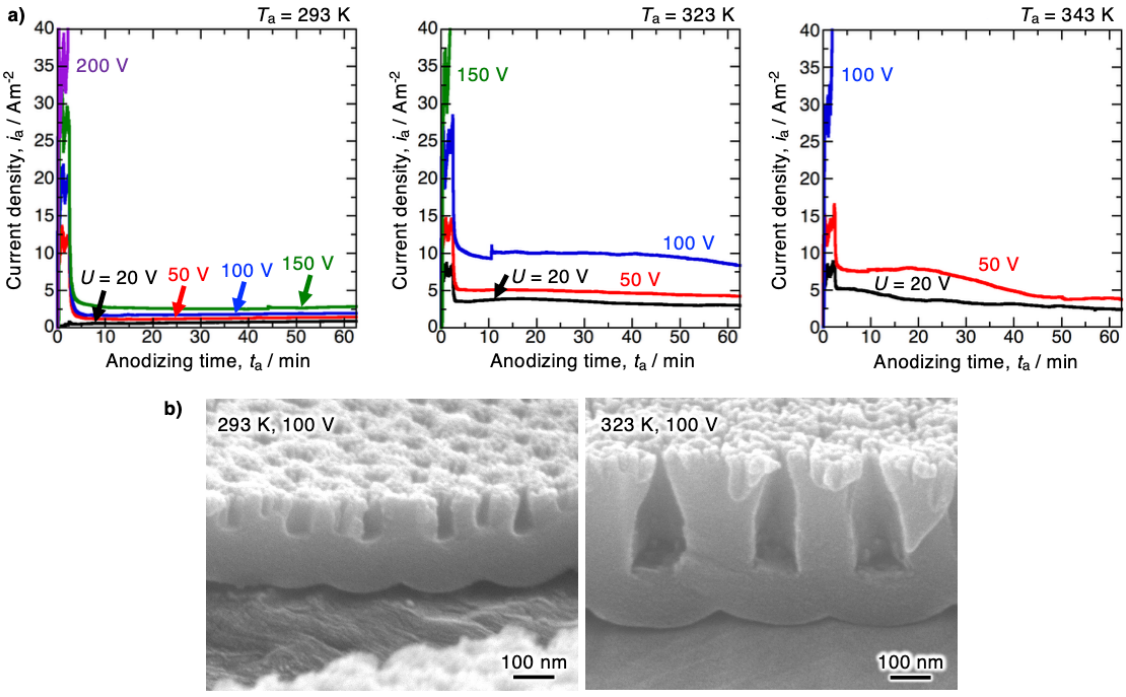
a)
T_a = 293 K
T_a = 323 K
T_a = 343 K
Current density, i_a / Am^{-2}
Anodizing time, t_a / min
200 V
150 V
100 V
50 V
U = 20 V
b)
293 K, 100 V
323 K, 100 V
100 nm

Figure 2.

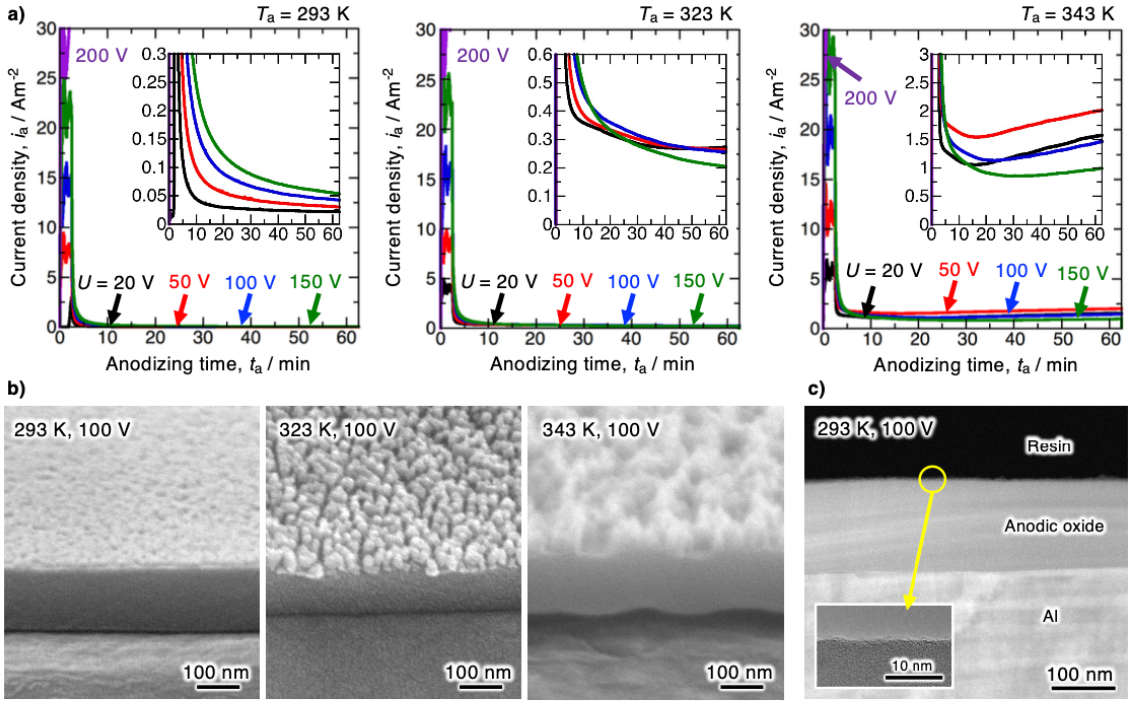
a)
T_a = 293 K
T_a = 323 K
T_a = 343 K
Current density, i_a / Am^{-2}
Anodizing time, t_a / min
200 V
U = 20 V 50 V 100 V 150 V
b)
293 K, 100 V
323 K, 100 V
343 K, 100 V
100 nm
c)
293 K, 100 V
Resin
Anodic oxide
Al
10 nm
100 nm

Figure 3.

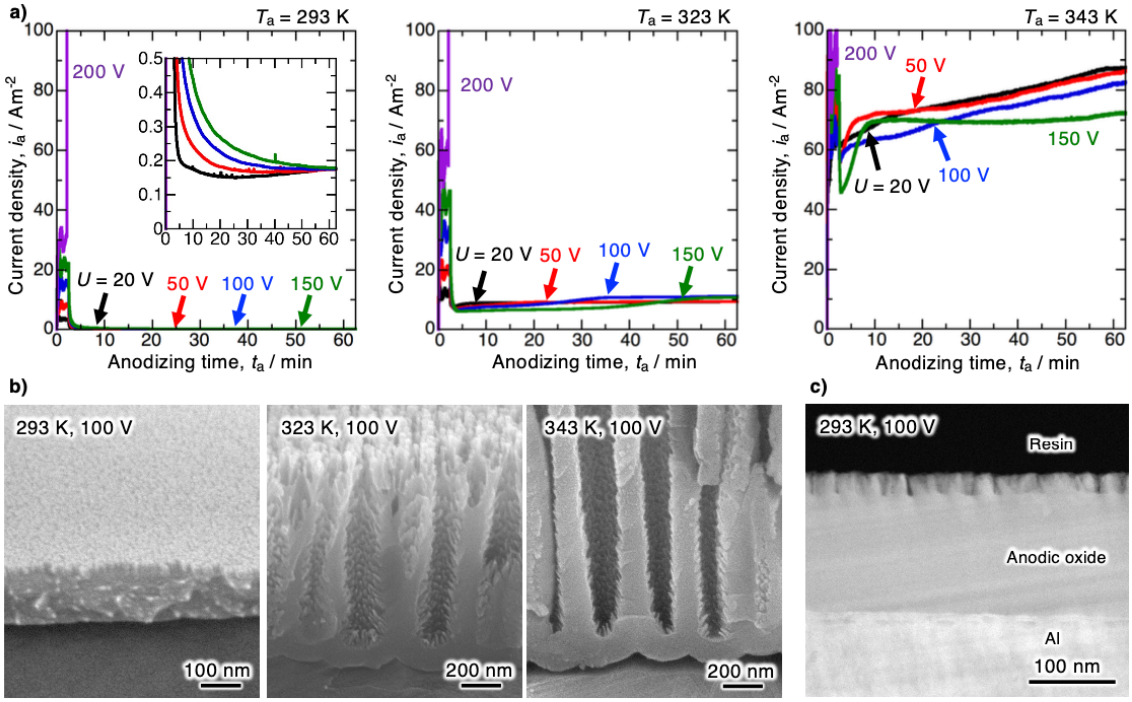
a)
T_a = 293 K
T_a = 323 K
T_a = 343 K
Current density, i_a / Am^{-2}
Anodizing time, t_a / min
200 V
50 V
100 V
150 V
U = 20 V
b)
293 K, 100 V
323 K, 100 V
343 K, 100 V
100 nm
200 nm
200 nm
c)
293 K, 100 V
Resin
Anodic oxide
Al
100 nm

Figure 4.

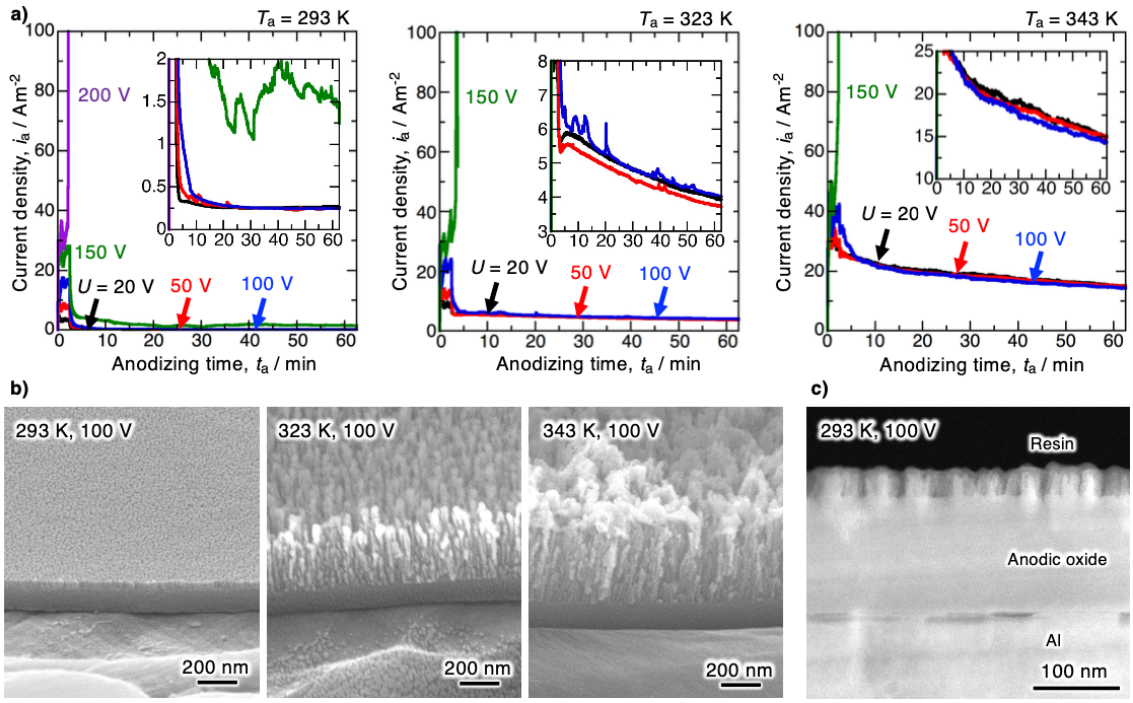
a)
T_a = 293 K
T_a = 323 K
T_a = 343 K
Current density, i_a / Am^{-2}
Anodizing time, t_a / min
200 V
150 V
U = 20 V
50 V
100 V
b)
293 K, 100 V
323 K, 100 V
343 K, 100 V
200 nm
c)
293 K, 100 V
Resin
Anodic oxide
Al
100 nm

Figure 5.

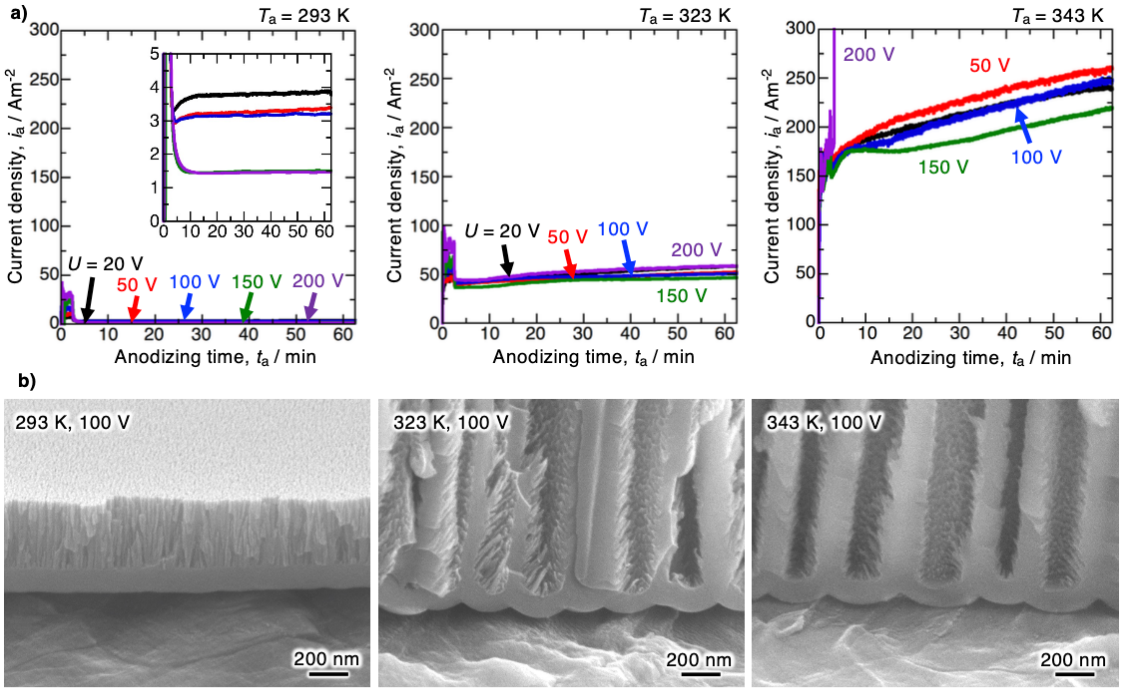
a)
T_a = 293 K
T_a = 323 K
T_a = 343 K
Current density, i_a / Am^{-2}
Anodizing time, t_a / min
U = 20 V
50 V
100 V
150 V
200 V
b)
293 K, 100 V
323 K, 100 V
343 K, 100 V
200 nm

Figure 6.

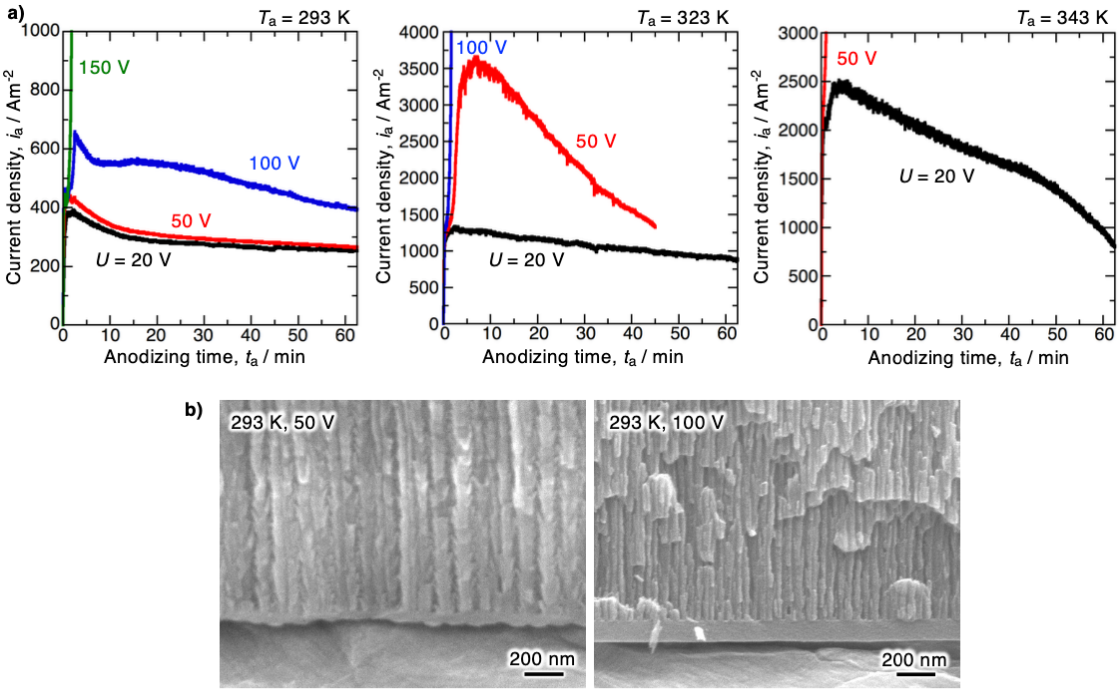
a)
T_a = 293 K
150 V
100 V
50 V
U = 20 V
Current density, i_a / Am^{-2}
Anodizing time, t_a / min
T_a = 323 K
100 V
50 V
U = 20 V
Current density, i_a / Am^{-2}
Anodizing time, t_a / min
T_a = 343 K
50 V
U = 20 V
Current density, i_a / Am^{-2}
Anodizing time, t_a / min
b)
293 K, 50 V
200 nm
293 K, 100 V
200 nm

Figure 7.

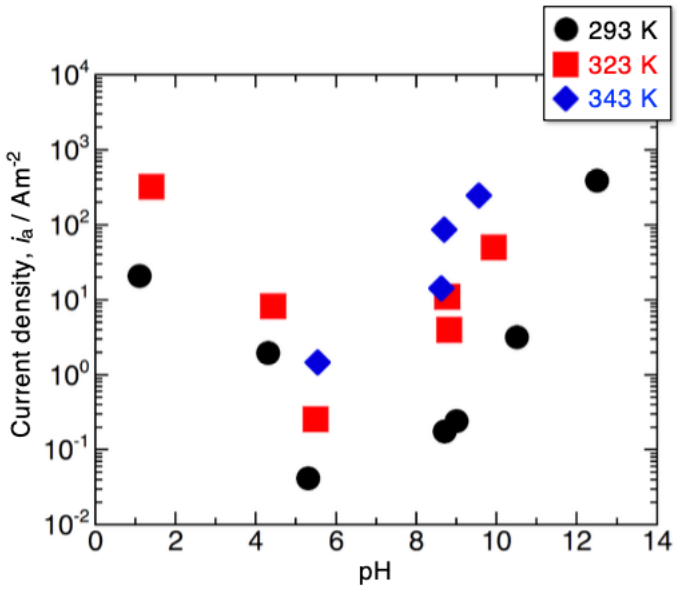
293 K
323 K
343 K
Current density, i_a / Am^{-2}
10^4
10^3
10^2
10^1
10^0
10^{-1}
10^{-2}
0
2
4
6
8
10
12
14
pH

Figure 8.

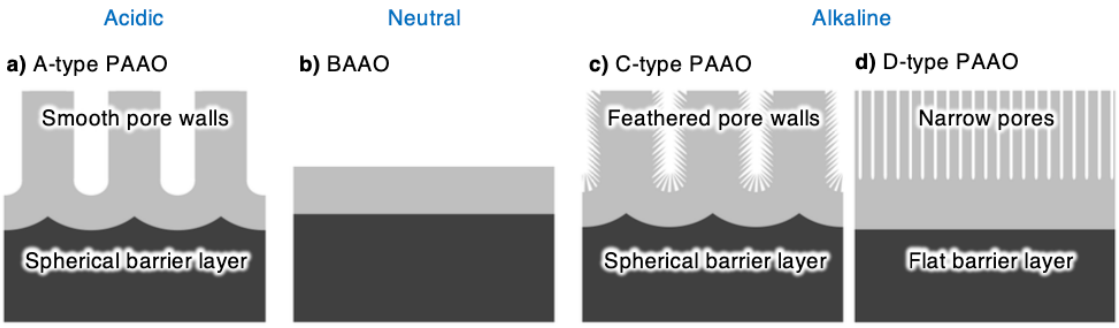
Acidic
Neutral
Alkaline
a) A-type PAAO
b) BAAO
c) C-type PAAO
d) D-type PAAO
Smooth pore walls
Spherical barrier layer
Feathered pore walls
Spherical barrier layer
Narrow pores
Flat barrier layer

Figure 9.

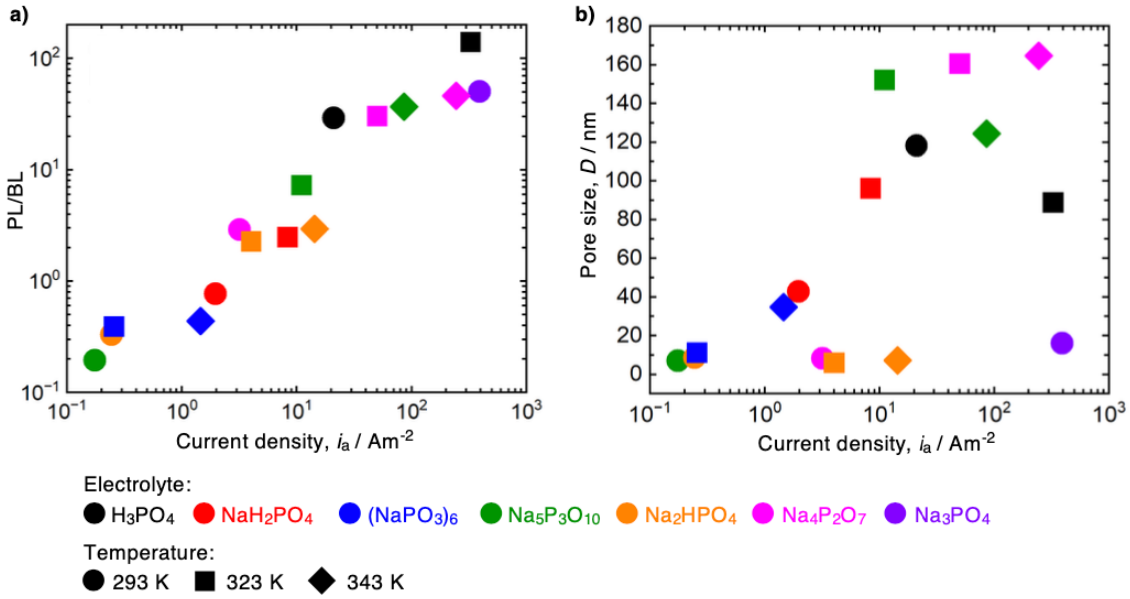
a)
PL/BL
Current density, i_a / Am^{-2}
b)
Pore size, D / nm
Current density, i_a / Am^{-2}
Electrolyte:
H_3PO_4 NaH_2PO_4 $(NaPO_3)_6$ $Na_5P_3O_{10}$ Na_2HPO_4 $Na_4P_2O_7$ Na_3PO_4
Temperature:
293 K 323 K 343 K

Figure 10.